# Identification of an Inhibitor Binding Site of Poly(ADP-ribose) Glycohydrolase†

David W. Koh,‡ Chandra N. Patel,‡ Sushma Ramsinghani,§ James T. Slama,§ Marcos A. Oliveira,‡,||,⊥ and Myron K. Jacobson*,@

*College of Pharmacy, Markey Cancer Center, and Center for Structural Biology, University of Kentucky, Lexington, Kentucky 40536, Department of Medicinal and Biological Chemistry, College of Pharmacy, University of Toledo, Toledo, Ohio 43606, and Department of Pharmacology and Toxicology, College of Pharmacy, and Arizona Cancer Center, University of Arizona, Tucson, Arizona 85724*

*Received November 20, 2002; Revised Manuscript Received February 18, 2003*

ABSTRACT: Polymers of ADP-ribose involved in the maintenance of genomic integrity are converted to free ADP-ribose by the action of poly(ADP-ribose) glycohydrolase (PARG). As an approach to mapping functions of PARG onto the amino acid sequence of the protein, we report here experiments that identify an amino acid residue involved in the binding of potent PARG inhibitors. A photoreactive inhibitor, [α-$^{32}$P]-8-azidoadenosine diphosphate (hydroxymethyl)pyrrolidinediol (8-$N_3$-ADP-HPD), was used to photolabel a recombinant bovine PARG catalytic fragment (rPARG-CF). N-Terminal sequencing of tryptic and subtilitic peptides of photoderivatized rPARG-CF identified tyrosine 796 (Y796), a residue conserved in PARG across a wide range of organisms, as a site of photoderivatization. Site-directed mutants where this tyrosine residue was replaced with an alanine residue (Y796A) had a nearly 8-fold decrease in catalytic efficiency ($k_{cat}/K_M$), while replacement with a tryptophan residue (Y796W) had little effect on catalytic efficiency. Surface plasmon resonance spectroscopy using the PARG inhibitor 8-(aminohexyl)amino-ADP-HPD demonstrated that the binding constant of the inhibitor for Y796A was 21-fold lower ($K_D$ = 170 nM) than that of wild-type PARG ($K_D$ = 8.2 nM), while Y796W displayed a binding affinity similar to that of the wild-type enzyme. Our results indicate that Y796 is involved in inhibitor binding to PARG via a ring stacking interaction and identify a highly conserved region of the protein that putatively contains other residues involved in catalytic activity and/or substrate recognition.

Poly(ADP-ribose)[1] glycohydrolase catalyzes the hydrolysis of the α(1″→2′) and α(1‴→2″) ribosyl−ribose linkages of ADP-ribose polymers to produce free ADP-ribose (*1*, *2*) (Figure 1). Since the enzymatic activity of this glycosyl hydrolase is unique within the cell, it is required for the completion of ADP-ribose polymer cycles initiated by poly(ADP-ribose) polymerases (PARPs) (*3*), a family of enzymes that catalyze the covalent modification of acceptor proteins with ADP-ribose polymers using nicotinamide adenine dinucleotide ($NAD^+$) as a substrate with the release of nicotinamide (*2*, *4*). ADP-ribose polymers can become very long and branched (*5*), and thus, polymer modification alters the structure and function of a number of DNA and chromatin binding proteins (*6*, *7*). ADP-ribose polymers are rapidly catabolized by PARG (*8*−*10*); thus, the activities of PARPs and PARG are closely coordinated.

The biological roles of ADP-ribose polymer cycles are emerging from studies of cellular PARPs. PARP-1, the original and most studied PARP, modulates cellular responses to genotoxic stress that can result in cellular recovery by facilitating DNA repair (*11*) and enhancing the degradation of damaged nuclear proteins (*12*), or cellular death by apoptosis (*13*, *14*) or necrosis (*15*). Because other PARPs have been linked to telomere maintenance (*16*) and nuclear transport (*17*), ADP-ribose polymer cycles appear to be involved in the maintenance of the genomic integrity in multiple ways. Characterization of cellular responses to genotoxic stress in the absence of PARP-1 activity (*18*−*20*) has led to the identification of PARP-1-initiated ADP-ribose polymer cycles as a potential therapeutic target for a number of conditions associated with genotoxic stress, including cancer (*21*), neurotoxicity (*18*), diabetes (*22*), and HIV infection (*23*). Because PARG has been shown to originate from a single-copy gene (*24*) with no other homologues identified to date, it is possible that it is required to complete polymer cycles initiated by many different PARPs. The potential of PARG as a therapeutic target has been suggested

† Supported by research grants from the American Cancer Society (85-001-13-IRG) and a Kentucky Lung Cancer Research Grant to M.A.O., grants from the Ohio Division of the American Cancer Society and de Arce Memorial Endowment Fund to J.T.S., and Grant CA 43894 from the National Institutes of Health to M.K.J.

* To whom correspondence should be addressed: Arizona Cancer Center, University of Arizona, 1515 N. Campbell Ave., Tucson, AZ 85724. Telephone: (520) 626-5957. E-mail: mjacobson@pharmacy.arizona.edu.

‡ College of Pharmacy, University of Kentucky.

§ University of Toledo.

|| Markey Cancer Center, University of Kentucky.

⊥ Center for Structural Biology, University of Kentucky.

@ University of Arizona.

[1] Abbreviations: ADP-HPD, adenosine diphosphate (hydroxymethyl)pyrrolidinediol; 8-$N_3$-ADP-HPD, 8-azidoadenosine diphosphate (hydroxymethyl)pyrrolidinediol; 8-AH-ADP-HPD, 8-(6-aminohexyl)amino-ADP-HPD; ADP-ribose, adenosine diphosphoribose; PARG, poly(ADP-ribose) glycohydrolase; bPARG, PARG purified from bovine thymus; rPARG-CF, recombinant bovine PARG catalytic fragment; DTT, dithiothreitol; SDS−PAGE, sodium dodecyl sulfate−polyacrylamide gel electrophoresis; PTH, phenylthiohydantoin; TFA, trifluoroacetic acid; RP-HPLC, reversed-phase HPLC.

10.1021/bi0272048 CCC: $25.00 
Published on Web 04/09/2003

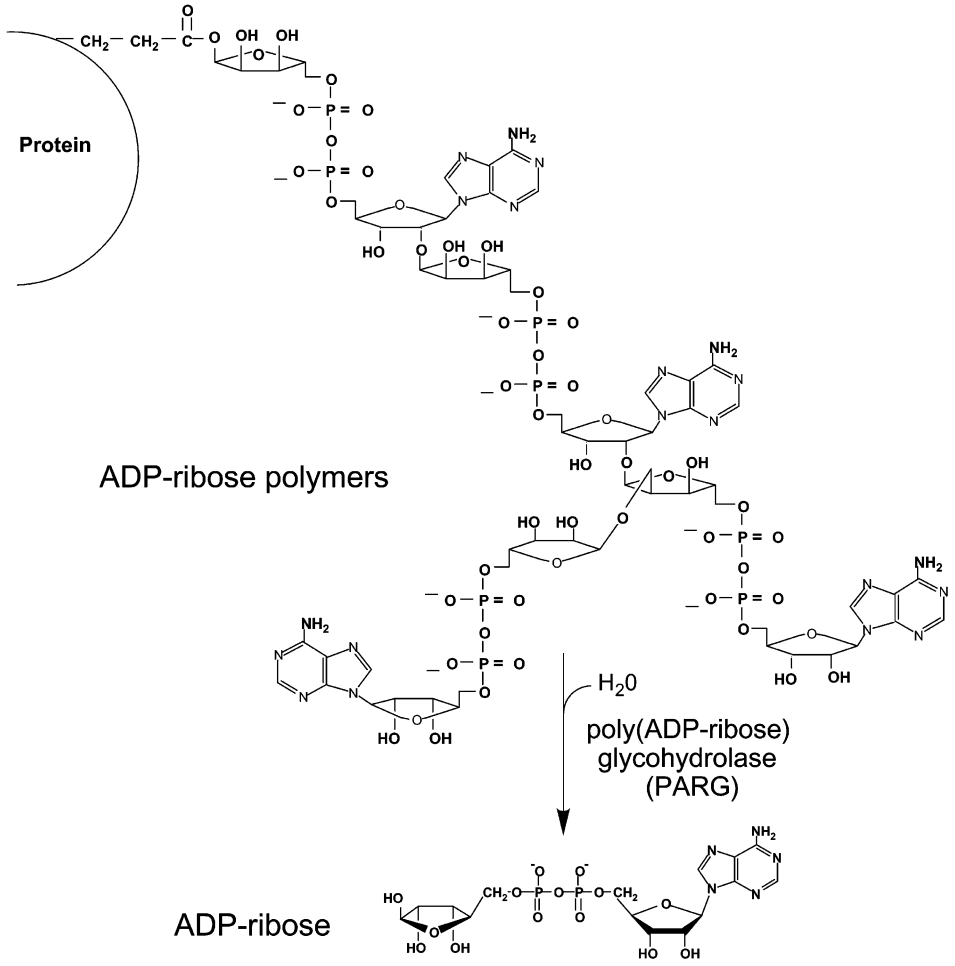


FIGURE 1: Structure of ADP-ribose polymers and hydrolysis catalyzed by PARG.

by the observation that the PARG inhibitor gallotannin inhibits PARP-1-mediated cell death in mouse neurons and astrocytes by slowing ADP-ribose polymer turnover and thus limiting $NAD^+$ depletion (*25*). In plants, a single point mutation within the PARG catalytic domain has been shown to affect the circadian rhythm (*14*).

Previous studies have identified adenosine diphosphate (hydroxymethyl)pyrrolidinediol (ADP-HPD, **1**), a nitrogen-in-the-ring analogue of ADP-ribose, as a potent and specific partial noncompetitive PARG inhibitor (*26*, *27*). The photoactive analogue of ADP-HPD, 8-azidoadenosine diphosphate (hydroxymethyl)pyrrolidinediol (8-$N_3$-ADP-HPD, **2**), was subsequently shown to specifically photoderivatize the ADP-HPD binding site of rPARG-CF (*28*). In this study, we utilized [$\alpha$-$^{32}$P]-8-$N_3$-ADP-HPD to photolabel rPARG-CF to identify binding residues and locate regions of the protein involved in substrate binding. A putative substrate binding residue was identified and confirmed by site-directed mutagenesis. Analysis of wild-type and mutant enzyme affinity for ligand by measurement using a surface plasmon resonance spectroscopy system further substantiated the role of this residue. As a result, this study provides the first insight into the structural details of PARG and its method of polymer recognition.

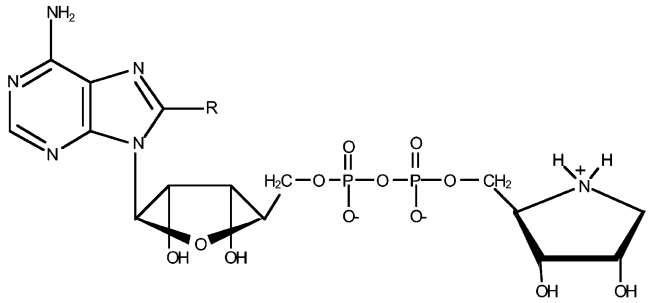

**1 : X=H**

**2 : X=$N_3$**

**3 : X=NH-$(CH_2)_6$-$NH_2$**

## EXPERIMENTAL PROCEDURES

*Materials*. [$\alpha$-$^{32}$P]-8-$N_3$-ADP-HPD at a specific activity of ~2 mCi/$\mu$mol was synthesized as described previously (*28*). Recrystallized urea and subtilisin were purchased from Boehringer Mannheim (Indianapolis, IN). 2-Iodoacetamide was obtained from Eastman Kodak Organic Chemicals (Rochester, NY). TPCK-treated trypsin was obtained from Worthington Biochemical Corp. (Lakewood, NJ). Matrex phenyl boronate agarose gel (PBA-30) was produced by Amicon (Beverly, MA). Ready gels (16.5% Tris-tricine gels with 4% stacking gels and 10 to 20% Tris-tricine gradient gels with 4% stacking gels) and molecular mass markers were obtained from Bio-Rad (Hercules, CA). Biomax MR-1 film for autoradiography was from Sigma Chemical Co. (St.

Louis, MO). Slide-A-Lyzer dialysis cassettes were from Pierce (Rockford, IL). Recombinant PARP (rePARP-1) was prepared as previously described (*29*), as was naturally occurring PARG isolated from bovine thymus (bPARG) (*30*), except that steps 6 (DNA-agarose) and 7 (heparin-Sepharose) were omitted and a Red-Sepharose step was added (*31*).

*Photolabeling of rPARG-CF*. All rPARG-CF was produced as a 1 mg/mL solution as previously described (*24*), incubated (8.2 nmol or 0.56 mg for tryptic digestion and 14.8 nmol or 1.0 mg for subtilitic digestion) with an equimolar amount of [$\alpha$-$^{32}$P]-8-$N_3$-ADP-HPD, and irradiated with short-wave UV light for 5 min at pH 7.4 using photolabeling conditions described previously (*28*). These conditions of photolabeling do not affect PARG enzymatic activity when the enzyme is irradiated in the absence of 8-$N_3$-ADP-HPD and the degree of photoderivatization is similar to the degree of inactivation of enzyme activity. For example, an experiment leading to 70% maximal photoderivatization resulted in the loss of 61% of PARG activity (data not shown). The photoderivatized protein was injected into a Slide-A-Lyzer dialysis cassette, and dialyzed against 500 mL of 100 mM ammonium bicarbonate (pH 8.5) for 2 h with one change in buffer. Radioactivity in an aliquot of the retentate was measured to ensure complete removal of excess unbound photolabel and decomposition products. The sample was then withdrawn from the dialysis cassette and transferred into a 1.5 mL Eppendorf tube.

*Digestion of Photolabeled rPARG-CF*. Prior to proteolytic fragmentation, the dialyzed solution of photolabeled rPARG-CF (0.7 mL for trypsin, 1.5 mL for subtilisin) was incubated in 8 M urea, 0.4 M ammonium bicarbonate, and 45 mM dithiothreitol (DTT) at 50 °C for 15 min with gentle shaking. After the mixture had cooled to room temperature for 15 min, 2-iodoacetamide was added to a final concentration of 0.1 M and the reaction mixture was incubated at room temperature in the dark for 15 min. The concentration of urea was then reduced to 2 M by addition of 3 volumes of diluent [water for trypsin and 0.1 M sodium borate (pH 8.0) for subtilisin]. For proteolytic digestion, *N*-tosyl-L-phenylalanine chloromethyl ketone-treated trypsin (5 wt % with respect to the weight of rPARG-CF in 1 mM HCl) or subtilisin (2% in 0.1 M sodium borate and 2 mM $CaCl_2$) was added, and the reaction solution was incubated at 37 °C in a shaking water bath for 8 h. A second addition of an equal amount of trypsin or subtilisin was made and the digestion continued overnight.

*Purification of Photolabeled Peptides for N-Terminal Sequencing*. Photolabeled and protease-digested rPARG-CF was initially purified by boronate affinity chromatography followed by reversed-phase HPLC (RP-HPLC) as previously described (*32*) with the following exceptions: 2−3 mL immobilized *p*-aminophenyl boronic acid column (PBA-30) as the boronate column, Vydac C4 reversed-phase column (4.6 mm × 150 mm, 10 $\mu$m, The Separations Group, Hesperia, CA) as the RP-HPLC stationary phase, initial RP-HPLC flow rate of 0.5 mL/min adjusted to 0.25 mL/min to facilitate maximum binding, and 2 mL fractions collected from RP-HPLC with radioactivity determined in 25−50 $\mu$L aliquots depending on the specific activity of the photolabel. Radioactive fractions collected for each step were pooled and concentrated to ∼1 mL *in vacuo* at ambient temperature on a centrifugal concentrator (Savant, Holbrook, NY). The final concentrate was dissolved in 10 $\mu$L of water, and the sample was submitted to peptide sequence analysis by the Edman degradation method (*33*).

*N-Terminal Amino Acid Sequence Analysis*. Fractions containing radioactivity which coincided with absorbance at 215 nm from reversed-phase HPLC were concentrated *in vacuo* at ambient temperature on a Savant centrifugal concentrator. The residue was dissolved in 10 $\mu$L of water and submitted to automated Edman degradation. N-Terminal amino acid sequence analysis was performed on an Applied Biosystem 477A pulsed liquid-phase protein sequencer with on-line identification of phenylthiohydantoin amino acids at the University of Kentucky Macromolecular Structure Analysis Facility (MSAF). Typically, many peaks were obtained in a single cycle that were isographic with standard PTH-amino acid derivatives. The amino acid in any given cycle was assigned at the facility on the basis of the picomole yield of a PTH-amino acid derivative and its increase in quantity over that in the previous cycle. The data reported for sequencing results are the identity assigned to the amino acid followed by the yield in picomoles of the assigned PTH-amino acid derivative in a cycle. ND denotes that assignment of an amino acid could not be made for that cycle.

Tryptic peptides: experiment 1 (41 min retention), L(59), F(53), T(24), E(31), V(24), L(19), and D(16); experiment 1 (43 min retention), L(99), F(81), T(55), E(42), V(71), L(56), D(22), H(7), N(13), E(10), S(6), L(10), I(22), I(29), T(5), G(17), T(7), E(6), and Q(5); and experiment 2 (43 min retention), L(49), F(47), T(23), E(13), V(33), L(25), D(4), H(1), N(3), E(4), ND, ND, I(27), I(39), T(2), and G(13).

Subtilisin-digested peptides: experiment 1 (23 min retention), S(46), E(36), Y(49), T(38), G(50), ND, and A(18); and experiment 2 (25 min retention), S(20), E(14), Y(15), T(14), G(26), ND, and A(5). All data for sequencing results are summarized graphically in Figure 4.

*Site-Directed Mutagenesis of Tyr-796.* The mutagenesis of Tyr-796 was carried out using the Quick Change site-directed mutagenesis kit (Stratagene). Two mutations were made: Y796A (Tyr-796 → Ala-796) and Y796W (Tyr-796 → Trp-796). The following forward and reverse complementary primers were designed to contain the desired mutations (underlined): Y796W, 5′-GAATACACAGGCTGGGCCGAAACATAC-3′ and 3′-CTTATGTGTCCGACCCGGCTTTGTATG-5′; Y796A, 5′-GAATACACAGGCGCGGCCGAAACATAC-3′ and 3′-CTTATGTGTCCGGCGCGGCTTTGTATG-5′.

The PCRs consisted of 50 ng of template DNA, 125 ng of each primer, 1 mM dNTP, and Stratagene reaction buffer (20 mM $MgSO_4$). High-fidelity PfuTurbo DNA polymerase (Stratagene) and 16 PCR cycles were used to reduce the chances of random mutations (*34*). The methylated template DNA was digested using *Dpn*I (Stratagene). After digestion, 5 $\mu$L of the PCR mixture was used to transform XL-1 Blue (Stratagene) competent cells. Clones were sequenced with upstream (5′-GGAAACGGCCAGGGCATGCTAC-3′) and downstream (3′-CTGCTGACCGTCTCCGCGTGC-5′) primers to verify approximately 200 bp around the mutation.

*Preparation and Characterization of Wild-Type rPARG and Tyrosine 796 Mutants.* The cloned plasmid containing the mutation was transformed into *Escherichia coli* NM522 cells and expressed and purified as previously described (*24*). The final products were quantified with the Bradford protein

Table 1: Enzyme Kinetic Parameters of Bacterially Expressed PARG Substitution Mutants Constructed by Site-Directed Mutagenesis of Tyr-796[a]

| rPARG-CF | rPARG-CF phenotype | $V_{max}$ ($\mu$mol min$^{-1}$ mg$^{-1}$) | $K_M$ ($\mu$M) | $k_{cat}$ (min$^{-1}$) | $k_{cat}/K_M$ (min$^{-1}$ $\mu$M$^{-1}$) |
|---|---|---|---|---|---|
| wild type | wild type | $2.6 \pm 0.2$ | $0.87 \pm 0.16$ | $156 \pm 12$ | $179 \pm 36$ |
| Y796A | Tyr-796 → Ala-796 | $0.43 \pm 0.05$ | $1.2 \pm 0.2$ | $28 \pm 3$ | $23 \pm 5$ |
| Y796W | Tyr-796 → Trp-796 | $4.4 \pm 0.5$ | $2.0 \pm 0.2$ | $280 \pm 32$ | $140 \pm 21$ |

[a] Kinetic data were generated using the PARG TLC assay and varying substrate concentrations as described in Experimental Procedures. Lineweaver−Burk plots were generated by SigmaPlot, and the remaining enzyme kinetic parameters were then calculated using the resulting statistical analyses. Data are expressed as means of values from several experiments with assays performed a minimum of three times.

assay, analyzed by SDS−PAGE, and stored at −80 °C until they were needed in phosphate-buffered physiological saline (PBS) (pH 7.2) containing 10% glycerol, 5 mM 2-mercaptoethanol, 0.1% Triton X-100, 5 mM EDTA, 1 mM PMSF, 100 $\mu$M antipain, and 2 $\mu$g/mL aprotinin. Enzymatic characterizations of each mutant via PARG activity assays was accomplished using the procedure previously reported by Ménard and Poirier with [$\alpha$-$^{32}$P]ADP-ribose polymers as a substrate (*35*), prepared at high specific activity from [$\alpha$-$^{32}$P]NAD$^+$ and rePARP using the procedure described by Kiehlbauch et al. (*36*), except that core histones (type IIA) were omitted from the incubation mixture. These conditions result in a heterogeneous mixture of long chain ADP-ribose polymers that also contain branching. Assays were run from 2 to 4 min using 2 ng of wild-type rPARG-CF, 2 ng of Y796W, or 8 ng of Y796A in a total volume of 30 $\mu$L. Substrate concentrations ranged from 1 to 12.5 $\mu$M [$\alpha$-$^{32}$P]-ADP-ribose polymers, and Lineweaver−Burk kinetic data were processed by Sigmaplot (SPSS Science).

*Surface Plasmon Resonance (SPR) Spectroscopy*. A BIAcore X biosensor (Biacore, Inc., Uppsala, Sweden) that measures surface plasmon resonance (SPR) was utilized to determine kinetic parameters for the interaction of wild-type rPARG-CF and Y796A and Y796W mutants (analytes) with an immobilized ADP-HPD analogue (ligand), 8-(6-aminohexyl)amino-ADP-HPD (8-AH-ADP-HPD), that was also characterized as a rPARG-CF inhibitor (unpublished observations). A standard amine coupling reaction was used (*37*) to attach the 8-AH-ADP-HPD to a research grade CM5 chip (BIAcore). The buffer consisted of 10 mM HEPES (pH 7.4), 150 mM NaCl, 3 mM EDTA, and 0.005% surfactant P20 (HBS-EP buffer). The immobilization was done by first activating the CM5 chip with a 2 min pulse of *N*-hydroxysuccinimide and *N*-ethyl-*N*′-(dimethylaminopropyl)carbodiimide (NHS/EDC). Following activation, the amine coupling was performed with a 7 min pulse of a 160 nM/$\mu$L solution of 8-AH-ADP-HPD. The chip was then inactivated by a 7 min ethanolamine wash. The immobilization procedure theoretically results in a maximum of 16% coupling of the carboxyl groups of the sensor chip.

For all SPR measurements, two flow cells were simultaneously utilized, one flow cell containing the 8-AH-ADP-HPD sensor chip and the second one containing the control surface with no inhibitor coupling, to obtain parallel measurements of the level of nonspecific binding. The result was a real-time reference subtraction, which effectively quantified the analyte−ligand interaction. Protein solutions containing wild-type or mutant enzyme in 40 $\mu$L of buffer [50 mM Tris-HCl (pH 7.5), 300 mM KCl, 10 mM 2-mercaptoethanol, and 0.1% Triton X-100] were diluted in HBS-EP buffer to final concentrations ranging from 10 to 500 nM, and then 40 $\mu$L was injected for analysis. Each experiment began with a 30 s pulse containing HBS-EP buffer to establish a baseline followed by a 90 s sample injection where the association phase is observed (Figure 6). After the association phase, HBS-EP buffer was injected for 300 s in an effort to observe the dissociation phase. At the end of each experiment, the CM5 chip was regenerated utilizing a 70−100 $\mu$L injection of 6 M urea and 0.1 M boric acid (pH 8.9) and 0.5 M NaCl. For each rPARG-CF sample, a set of sensorgrams was recorded at several different protein concentrations in the range of 14−100 nM. The kinetic parameters were obtained using nonlinear least-squares global fitting of three to five independent experiments at different protein concentrations and analyzed using the BIAevaluation version 3.1 software. The observed data were fitted to a single interaction model from which the association rate constant ($k_a$) and the dissociation rate constant ($k_d$) were determined and utilized to calculate the equilibrium dissociation constant ($K_D$). The estimate of error is given by $\chi^2$ which represents the mean square of the difference between observed and fitted association and dissociation curves (Figure 6). The $\chi^2$ values for the experiments reported in Table 2 were less than 6 (BIAcore evaluation handbook, version 3.0). The net change in Gibbs free energy ($\Delta\Delta G$) for mutant rPARG-CF relative to WT rPARG-CF was also calculated.

Table 2: Parameters for Binding of the Inhibitor ADP-HPD to Wild-Type PARG and Mutants Targeting the Photolabeled Tyrosine 796[a]

| rPARG-CF | $k_a$ (M$^{-1}$ s$^{-1}$) | $k_d$ (s$^{-1}$) | $K_D$ (nM) | $\Delta\Delta G$ (kcal/mol) |
|---|---|---|---|---|
| wild type | $4.3 \times 10^5$ | $3.6 \times 10^{-3}$ | 8.2 | − |
| Y796A | $9.8 \times 10^4$ | $1.7 \times 10^{-2}$ | 170 | 1.795 |
| Y796W | $6.3 \times 10^5$ | $2.1 \times 10^{-3}$ | 3.3 | −0.538 |

[a] The kinetic parameters were obtained using nonlinear least-squares global fitting of three to five independent experiments at different protein concentrations. The observed data were fitted to a single-site interaction model. This gave the association rate constant ($k_a$) and the dissociation rate constant ($k_d$), which then gave the equilibrium dissociation constant ($K_D$). The estimate of error is given by $\chi^2$ which represents the mean square of the difference between the observed and fitted curve. The $\chi^2$ values were below 6 for the data reported in this table (BIAcore evaluation handbook, version 3.0, 1997).

## RESULTS

*Photolabeling and Digestion of rPARG-CF*. The rPARG-CF was photolabeled by irradiation in the presence of a low concentration of [$\alpha$-$^{32}$P]8-N$_3$-ADP-HPD and then dialyzed against 100 mM ammonium bicarbonate (pH 8.5). The radioactivity in the retentate represented 13−17% of the initial radioactivity of the photoprobe and was similar to photoincorporation yields in small-scale experiments (*28*). This ensured that the unbound photolabel and decomposition products were removed effectively by dialysis. Photolabeled

rPARG-CF was treated with 45 mM DTT in the presence of 8 M urea and modified by carboxamidomethylation with 100 mM 2-iodoacetamide (*38*, *39*). SDS−PAGE followed by autoradiography after treatment showed that the band at an $M_r$ of 65 000 retained the radiolabel, indicating that the photoderivatized rPARG-CF did not lose the photolabel under conditions of reductive alkylation. The concentration of urea was lowered to 2 M, and the protein was digested with TPCK-treated trypsin for 18 h. SDS−PAGE of digested product revealed a diffuse radioactive band isographic with a 17 kDa molecular mass marker protein. Alternatively, when proteolysis was catalyzed by the unspecific endopeptidase subtilisin, a photolabeled peptide with a lower apparent molecular mass was obtained.

*Purification of Photoderivatized Peptides for Sequence Analysis.* The photolabeled peptides generated by digestion of modified rPARG-CF with either trypsin or subtilisin were initially purified by immobilized boronate affinity chromatography. Photolabeled peptides specifically retained on the column at pH 8.9 were eluted in buffer containing the competing polyalcohol sorbitol. A typical radioactivity profile obtained from the isolation of photolabeled peptides from tryptic digestion (Figure 2A) and subtilitic digestion (Figure 2B) is shown. Most of the radioactivity remained bound to the column until the application of sorbitol.

The sorbitol concentrate from immobilized boronate affinity chromatography was further purified by C4 RP-HPLC. Figure 3 shows the chromatogram associated with photolabeled peptides obtained by proteolysis. In the case of both tryptic and subtilitic digestions, the bulk of the radioactivity eluted at the beginning of the gradient corresponding to a major peak of absorbance. This position in the chromatogram corresponded to an elution time coincident with the void volume of the column. This peak was also isographic with photoprobe that had been irradiated in water (data not shown). Radioactivity in the leading fraction that is not associated with peptide is seen frequently in photolabeling studies (*40*). In the case of the trypsin-digested sample, the fractions containing this leading radioactive peak were pooled, concentrated, and submitted to sequence analysis. No peptide sequence was obtained, and therefore, this peak was assumed to be nonpeptidyl. A likely cause for this early peak of radioactivity is the instability of the bond between the photoinserted nucleotide and the modified amino acid residue under the conditions of HPLC analysis. We investigated the cause of this instability by subjecting a photoderivatized protein to conditions of digestion and purification (data not shown). We found that the photoadduct was stable under the conditions used for reduction and carboxymethylation, boronate affinity purification, and the acidic conditions of HPLC when these conditions were employed individually. However, a significant amount of the photolabel (~72%) was lost when the photolabeled rPARG-CF was subjected to the conditions of reduction and carboxymethylation followed by the acidic conditions of HPLC. As a result of this instability, accurate quantification of the label present in HPLC-purified peptides was not possible.

A single radioactive peak from tryptic digestion eluted about midway in the gradient (Figure 3, trypsin digest, panel B). Portions of the material eluting at 41 and 43 min were concentrated separately and submitted for N-terminal amino acid sequence analysis. In a repeat experiment, the material

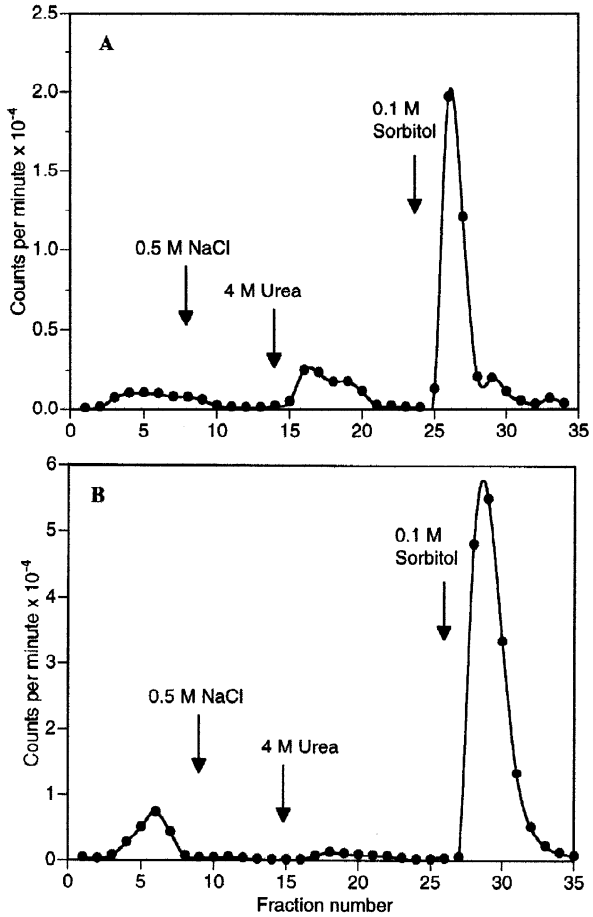


FIGURE 2: Isolation of photolabeled peptides from tryptic or subtilitic digestion by boronate affinity chromatography. Peptides from tryptic digestion (A) or subtilitic digestion (B) of photolabeled rPARG-CF were applied to an immobilized boronate PBA-30 affinity column (2−3 mL) equilibrated in buffer A [0.1 M ammonium acetate (pH 8.9)]. Chromatography was carried out by sequential application of 10 mL each of buffer A, buffer A containing 0.5 M NaCl, buffer A containing 4 M urea, and finally buffer A to elute non-photolabeled peptides. The photolabeled peptides were eluted into 20 mL of buffer A containing 0.1 M sorbitol. Fractions (1.5 mL) were collected, and the radioactivity of aliquots was quantified by liquid scintillation counting.

eluting at 43 min was sequenced. For the subtilisin digestion, the radioactive material eluting at approximately 23 min (Figure 3, subtilisin digest, panel B) was concentrated and submitted for sequence analysis. In a duplicate experiment, the radioactive peak had a retention time of 25 min (data not shown) and was submitted for sequence analysis.

*N-Terminal Amino Acid Sequence Analysis.* The major radioactive peak purified from the tryptic digestion of the photoadduct eluting at 43 min (Figure 3) was sequenced successfully through 19 cycles beginning with Leu through Gln (Figure 4). The peak with a retention time of 41 min contained less peptide and could only be sequenced through seven cycles, but revealed the same N-terminal sequence. The photolabeled peptides obtained from each subtilisin digestion sequenced through seven cycles beginning with Ser and ending with Ala (Figure 4). A PTH derivative could not be identified in cycle 6 of either sequence analysis, indicating that this residue was the probable site of photomodification. Sequence analysis of photolabeled tryptic and subtilitic peptides showed that each corresponding radioactive peak contained only a single peptide since a single product was

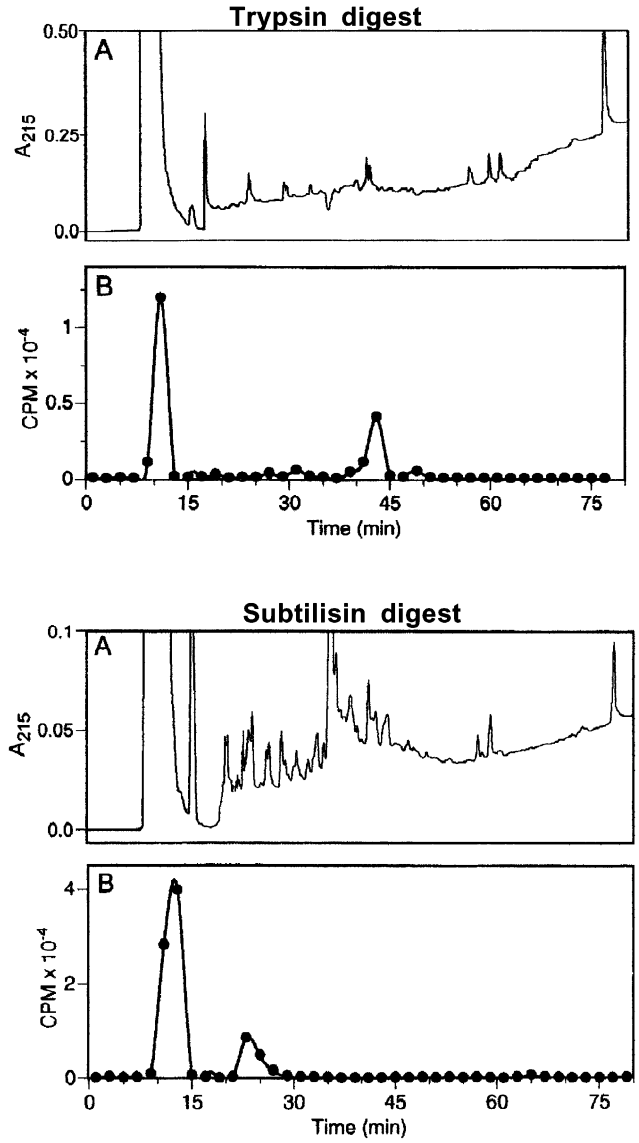


FIGURE 3: Purification of photolabeled peptides by HPLC. Fractions of radiolabeled peptides from boronate affinity chromatography were pooled, concentrated to 1 mL, and applied to a $C_4$ RP-HPLC column (4.6 mm × 150 mm, 10 $\mu$m) pre-equilibrated in 100% buffer A [0.1% (v/v) TFA]. Chromatography was carried out at 0.25 mL/min for 10 min at 100% A followed by a linear gradient over the course of 70 min to 100% B [0.1% (v/v) TFA in 70% (v/v) acetonitrile] at 1 mL/min. Fractions (2 mL) were collected, and the radioactivity of an aliquot was measured by liquid scintillation counting: (A) absorbance at 215 nm and (B) radioactivity in counts per minute.

assigned for each cycle. Further, N-terminal amino acid sequencing of the tryptic and subtilitic peptides identified a region that maps near the C-terminus of the deduced bPARG amino acid sequence (Figure 4). Because each proteolytic digest of photolabeled rPARG-CF ultimately mapped to this region, it was highly probable that this region represented, or at least constituted a portion, of the PARG inhibitor binding site. As a result, it was also highly probable that one or more amino acid residues directly involved in substrate recognition were contained in this region.

*Site-Directed Mutagenesis of Tyr-796 in rPARG-CF*. With the potential significance of Tyr-796 identified through photoaffinity labeling, we tested the hypothesis that bPARG initially binds to substrate through an interaction of Tyr-796 with an adenine moiety of ADP-ribose polymers. Site-directed mutagenesis of the bPARG amino acid sequence was utilized to transform Tyr-796 into alanine (Y796A) or tryptophan (Y796W). The tryptophan mutant was predicted to facilitate the interaction of PARG and ligand and therefore give the smallest deviations from wild-type enzymatic parameters. The expression and purification of the rPARG-CF mutants were accomplished as previously described with wild-type rPARG-CF (*24*). The final products appeared to be highly pure as determined by SDS−PAGE (Figure 5, lanes 3−5), and comparable in size to bPARG isolated from bovine thymus. The purified rPARG-CF clones were then assayed to determine kinetic parameters for each to ascertain the effect of the site-directed mutagenesis (Table 1). The $K_M$ value of 0.87 $\mu$M for wild-type rPARG-CF was the lowest of all the clones, demonstrating that it has the highest affinity for ADP-ribose polymers. $K_M$ values of 2.0 and 1.2 $\mu$M were measured for Y796W and Y796A, respectively. Interestingly, the $K_M$ for Y796A was more comparable to that of wild-type rPARG-CF than that of Y796W. The catalytic efficiency ($k_{cat}/K_M$) was highest for the wild type (179 $min^{-1}$ $\mu M^{-1}$) and lowest for Y796A (22 $min^{-1}$ $\mu M^{-1}$), which represents a nearly 88% decrease. Furthermore, the $k_{cat}/K_M$ value of 140 $min^{-1}$ $\mu M^{-1}$ for Y796W was comparable to that of the wild type. In summary, site-directed mutagenesis of Tyr-796 revealed that Y796W was the most efficient mutant while Y796A displayed a decrease in catalytic efficiency.

*Surface Plasmon Resonance Spectroscopy of Wild-Type rPARG-CF and Mutants*. The affinity of wild-type and site-directed mutants of rPARG-CF for the 8-aminohexyl derivative of ADP-HPD (8AH-ADP-HPD, **3**) was analyzed by assessing protein binding to the immobilized ligand. Sensorgrams were obtained from injection of the wild-type, Y796A, and Y796W enzyme onto chip surfaces coated with 8-AH-ADP-HPD. The sensorgram obtained for wild-type rPARG-CF binding to the 8-AH-ADP-HPD ligand immobilized in the CM5 chip is shown in Figure 6. The smooth lines represent best-fit plots for a single-site binding model of enzyme−ligand interaction with mass transfer. Global fitting of the sensorgrams to a single-site interaction model yielded association and dissociation rates and equilibrium dissociation constants, from which the change in the Gibbs free energy for binding was calculated as presented in Table 2. These values were estimated on the basis of at least three independent experiments made on the same sensor chip with estimation of error as determined by $\chi^2$ analysis. The $k_a$ and $k_d$ values calculated for the wild-type enzyme were $4.3 \times 10^5$ $M^{-1}$ $s^{-1}$ and $3.6 \times 10^{-3}$ $s^{-1}$, respectively. The corresponding dissociation equilibrium constant ($K_D$), as calculated from the association ($k_a$) and dissociation rate constants ($k_d$), was approximately 8.2 nM, which indicated a high level of affinity of wild-type rPARG-CF for 8-AH-ADP-HPD. In contrast, the $k_a$ value of $9.8 \times 10^4$ $M^{-1}$ $s^{-1}$ for Y796A was approximately 4.4-fold lower than that of the wild type, while the corresponding $k_d$ value was $1.7 \times 10^{-2}$ $s^{-1}$, or 4.7-fold higher than that of the wild type. However, the magnitude of the decrease in affinity of Y796A for 8-AH-ADP-HPD was most clearly illustrated by the $K_D$ value (170 nM) that is 21-fold higher than the wild-type value, and an energetically unfavorable increase in Gibbs free energy ($\Delta\Delta G$ = +1.795 kcal/mol) as compared to the wild-type binding

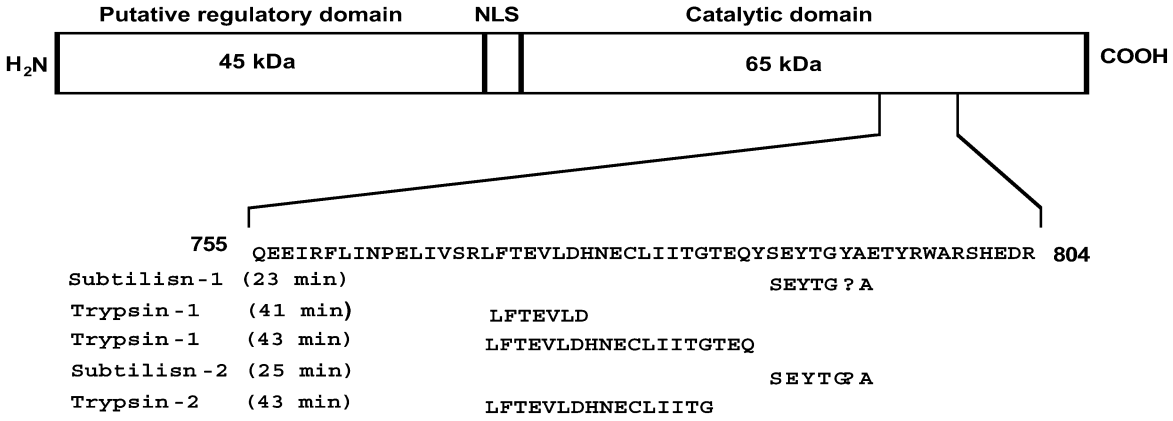


FIGURE 4: Partial sequence of rPARG-CF delineating the photoderivatized region. The sequence of the photolabeled peptide in a portion of the catalytic domain of bPARG is shown. In duplicate experiments, tryptic peptides were sequenced from Leu-771 to Gln-789 and from Leu-771 to Gly-786. For subtilisin, the peptides obtained from duplicate experiments consisted of Ser-791−Ala-797. Tyr-796 is proposed to be the site of photomodification.

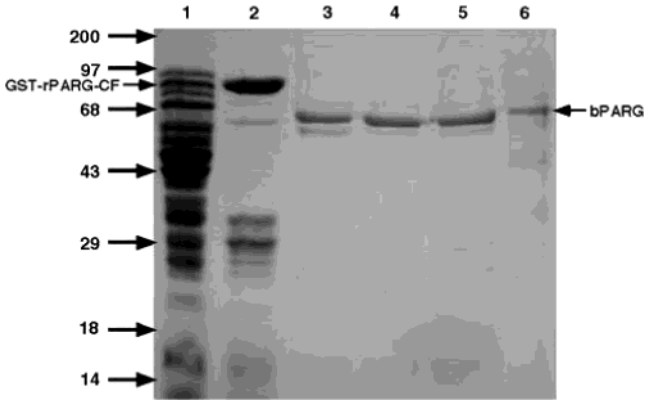


FIGURE 5: Expression and purification of rPARG mutants. Each rPARG-CF mutant was prepared as previously described (*15*). A 12% SDS−PAGE gel was run at 150 mV with molecular mass markers indicated by the arrows at the left: lane 1, 50 $\mu$g of wild-type rPARG-CF crude extract containing the GST−rPARG fusion (arrow); lane 2, 15 $\mu$g of wild-type rPARG-CF cell extract proteins bound to GSH-Sepharose; and lanes 3−6, 5 $\mu$g of wild-type rPARG-CF, 5 $\mu$g of Y796A, 5 $\mu$g of Y796W, and 2 $\mu$g of bPARG, respectively (all final products released by thrombin from the corresponding rPARG-CF cell extracts).

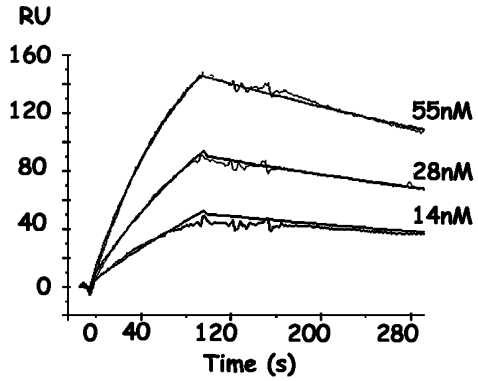


FIGURE 6: Plot of the observed interaction sensorgram from the BIAcore X instrument. The plot shows the interaction of three different concentrations (14, 28, and 55 nM) of wild-type PARG with a CM-5 chip where 8-AH-ADP-HPD has been immobilized. The jagged lines represent the actual data from three independent experiments, and the smooth lines are a fit of a single-site interaction model with mass transfer.

reaction. Interestingly, Y796W had a binding constant similar to that of the wild type for 8-AH-ADP-HPD.

## DISCUSSION

The involvement of ADP-ribose polymer cycles in the maintenance of genomic integrity raises the interesting possibility that the metabolic enzymes involved in this metabolism may represent targets for the development of new therapy for conditions where genomic integrity is altered. Little is known regarding the mechanism of action of PARG, except that it contains both endo- and exoglycosidic activities (*41*, *42*). In the study presented here, we have used [$\alpha$-$^{32}$P]8-$N_3$-ADP-HPD to map an amino acid within the bPARG catalytic domain that is involved in inhibitor binding. Further, we have confirmed the involvement of this residue in inhibitor binding by site-directed mutagenesis and surface plasmon resonance binding analyses.

Analysis of photolabeled tryptic or subtilitic peptides by RP-HPLC yielded two major radioactive peaks. The peak eluting at the beginning of the gradient (~11 min, Figures 3) was nonpeptidyl as determined by sequence analysis. This is common in photolabeling studies (*40*), and a likely cause is the instability of the bond between the photoinserted nucleotide and the modified amino acid residue under the HPLC conditions. As a result, a large portion of the radioactive photomodified label may be lost upon initial binding of the photolabeled peptide to the column and elute into the void volume (*43*). Thus, we cannot rule out the possibility that amino acid residues other than the one that we have identified are also involved in binding ADP-HPD. It is possible that the site of photoderivatization that we have characterized in this study is only a minor site of modification. This possibility dictated the independent approaches discussed below to verifying that the site of stable modification we observed was involved in the binding of ADP-HPD to the enzyme.

All the tryptic peptides had the same N-terminal amino acid sequence beginning with Leu (Figure 4). Upon searching the amino acid sequence of bPARG (*24*), we found that the amino acid sequence of our photolabeled tryptic peptide corresponded to a sequence of residues in bPARG beginning from Leu-771 (Figure 4). This sequence was consistent with tryptic digestion since the preceding amino acid is arginine, but the entire tryptic peptide would be expected to extend at least through Arg-801 (Figure 4). The inability to obtain additional sequence analysis was limited by the small

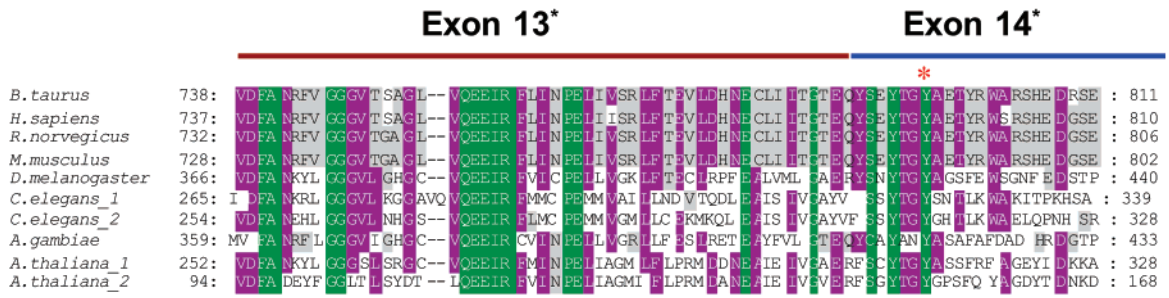


FIGURE 7: Comparison of PARG amino acid sequences from different species. The amino acid sequence in the photoderivatized region of bovine PARG (bPARG) was aligned with nine additional PARG sequences across a wide range of organisms. The gene structure of PARG to be reported elsewhere shows exon 13 and a portion of exon 14. Residues shown in green represent sequence identity in all 10 sequences. Residues shown in purple show identity in at least five of the 10 sequences. Residues shown in gray represent conservation of residues in vertebrate sequences. The proposed site of photolabeling is shown with an asterisk. The accession numbers for PARG are as follows: AAB5337 for *Bacillus taurus*, AAB61614 for *Homo sapiens*, AAC28735 for *Mus musculus*, BAA87901 for *Rattus norvegicus*, AAC28734 for *Drosophila melanogaster*, AAF39896 for *Caenorhabditis elegans* (arbitrary 1), T21138 for *C. elegans* (arbitrary 2), AF294690 for *Arabidopsis thaliana*_1, and AAC61937 for *A. thalia*_2.

amounts of photolabeled peptide that could be obtained. Nonetheless, tryptic digestion of the photolabeled protein enabled us to identify the region of photoderivatization, a 30-amino acid residue peptide (Leu-771−Arg-801) in a primary sequence of 977 amino acids of bPARG-CF. The subtilitic peptide sequence corroborated these results by identifying a region from Ser-791 to Ala-797 (Figure 4). Thus, both tryptic and subtilitic digestion of photolabeled rPARG-CF identified photolabeled peptides in the same region of PARG.

Tyrosine at position 796 is the likely site of photochemical modification by the photoprobe since it was not detected in the sequencing experiments. The repeated ability to specifically photolabel rPARG-CF at Tyr-796 and the fact that the reactive azido group of the photoprobe was at position 8 of adenine suggested a direct interaction of Tyr-796 and the adenine moiety of the inhibitor. It was therefore predicted that PARG binds ADP-HPD through the interaction between Tyr-796 and the adenine unit of the inhibitor through a ring stacking interaction. This view is supported by the tryptophan substitution (Y796W) which was able to replace tyrosine, showing little effect on the $k_{cat}/K_M$ of rPARG-CF (Table 1). The alanine mutation at position 796 was designed to reduce the extent of interaction with ADP-HPD binding by removing the ring stacking interaction. This mutation caused an approximately 9-fold decrease in $k_{cat}/K_M$, affecting both $K_M$ and $k_{cat}$. Although the $K_M$ value of 1.2 $\mu$M for Y796A was not as high as one might expect, the precipitous reduction in $k_{cat}/K_M$ for this mutant suggests that position 796 is mapping to a polymer binding subsite that, although causing little effect on the overall binding of the polymer, is likely acting at a distance affecting the stereochemistry at the catalytic site.

Substrate recognition for PARG is likely a complex event since PARG is able to cleave branched ADP-ribose polymers by both endo- and exoglycolitic mechanisms. Thus, it is likely that multiple attachment points or subsites for polymer recognition complicate any interpretation of $K_M$. While alterations in one subsite may interfere with the binding of the inhibitor 8H-ADP-HPD, it will not necessarily interfere with the ability of PARG to recognize polymers as a whole. At present, we do not know if ADP-HPD has a differential effect on the endo- and exoglycolitic activities or if it affects the processivity of the enzyme. Analogy with glycosyl hydrolases, which also catalyze hydrolysis of polymeric substrates, suggests that the active site topology of PARG may contain a tunnel or cleft allowing the binding of multiple units of ADP-ribose surrounding the labile O-glycosidic bond (*44*).

To augment Michaelis−Menten kinetic analyses discussed above, surface plasmon resonance spectroscopy was utilized to determine the binding affinity of the subsite mapped by 8-AH-ADP-HPD. Wild-type rPARG-CF was demonstrated to bind 8-AH-ADP-HPD with high affinity ($K_D$ = 8.2 nM); Y796A binding was 21-fold weaker ($K_D$ = 170 nM) with a binding that was more energetically expensive (+1.8 kcal/mol) than that of the wild type. Y796W was predicted to display the least deviant binding affinity for ligand among the mutants, which was observed in the Michaelis−Menten analysis (Table 1) and in binding analysis of Y796W binding to immobilized 8-AH-ADP-HPD (Table 2). This suggests that a hydrophobic ring stacking interaction plays an important role in the adenine recognition and tryptophan through the indole ring is able to form an effective interaction with the adenine ring of the inhibitors.

An interesting feature of our results is that the magnitude of the effects of the site-directed mutation is greater for inhibitor binding than for $K_M$ effects on enzyme activity. As Jenks has pointed out, a "fundamental distinction" between enzymes and simple small molecule catalysis is the ability of enzymes to utilize interactions remote from the active site to stabilize the transition state through substrate destabilization in which binding groups steer substrate into the proper stereochemistry. Our results are consistent with this view in that we have mapped an adenine binding pocket (Y796), likely distant from the site of O-glycosidic cleavage. Local perturbations at Y796 that show little effect on the overall binding of the ADP-ribose polymer ($K_M$) show a large effect on the binding of the 8AH-ADP-HPD inhibitor subsite. These local changes translate into differences in the catalytic power ($k_{cat}/K_M$) of PARG. The alanine mutation interferes specifically with the 8-AH-ADP-HPD subsite (21-fold increase in $K_D$, Table 2) with little effect on the overall polymer binding ($K_M$, Table 1). It appears that the detrimental local changes in this case are responsible for the major drop in catalytic efficiency (Table 1). Y796W on the other hand has a tighter interaction with 8-AH-ADP-HPD and an ~2-fold increase in $K_M$ with a small decrease in catalytic power (Table 1). In

the case of Y796W, the tighter interaction with 8-AH-ADP-HPD may be compensating for the poorer polymer binding (higher $K_M$), helping the enzyme to retain the necessary stereochemistry of the labile O-glycosidic bond at the distant catalytic site.

A comparison of 10 PARG sequences across a wide range of organisms revealed that Tyr-796 is conserved in all of these PARG sequences (Figure 7). Indeed, this region of the protein contains 15 other residues that are invariant across these organisms. This sequence identity includes another tyrosine residue that is three residues toward the amino terminus from Tyr-793. Taken together, the strong sequence homology provides further support for the notion that this region of PARG represents a portion of the active site of the enzyme. Thus, the results of this study should prove to be useful for identification of other residues of PARG involved in substrate binding and/or catalytic activity.

## ACKNOWLEDGMENT

All N-terminal sequencing was performed at the University of Kentucky Macromolecular Structure and Analysis Facility (MSAF) directed by Dr. Carol Beach. The BiaCore X instrument that was used is a core facility instrument from the Markey Cancer Center of the University of Kentucky.

## REFERENCES

1. Miwa, M., Tanaka, M., Matsushima, T., and Sugimura, T. (1974) *J. Biol. Chem. 249*, 3475−3482.
2. de Murcia, G., and Shall, S. (2000) Oxford Press, New York.
3. Jacobson, M. K., and Jacobson, E. L. (1999) *Trends Biochem. Sci. 24*, 415−417.
4. Adamietz, P. (1987) *Eur. J. Biochem. 169*, 365−372.
5. Alvarez-Gonzalez, R., and Jacobson, M. K. (1987) *Biochemistry 26*, 3218−3224.
6. Dantzer, F., Nasheuer, H. P., Vonesch, J. L., de Murcia, G., and Menissier-de Murcia, J. (1998) *Nucleic Acids Res. 26*, 1891−1898.
7. Adamietz, P., and Rudolph, A. (1984) *J. Biol. Chem. 259*, 6841−6846.
8. Juarez-Salinas, H., Sims, J. L., and Jacobson, M. K. (1979) *Nature 282*, 740−741.
9. Wielckens, K., Schmidt, A., George, E., Bredehorst, R., and Hilz, H. (1982) *J. Biol. Chem. 257*, 12872−12877.
10. Alvarez-Gonzalez, R., and Althaus, F. R. (1989) *Mutat. Res. 218*, 67−74.
11. Satoh, M. S., and Lindahl, T. (1992) *Nature 356*, 356−358.
12. Ullrich, O., Reinheckel, T., Sitte, N., Hass, R., Grune, T., and Davies, K. J. (1999) *Proc. Natl. Acad. Sci. U.S.A. 96*, 6223−6228.
13. Kaufmann, S. H., Desnoyers, S., Ottaviano, Y., Davidson, N. E., and Poirier, G. G. (1993) *Cancer Res. 53*, 3976−3985.
14. Panda, S., Poirier, G. G., and Kay, S. A. (2002) *Dev. Cell 3*, 51−61.
15. Berger, N. A. (1985) *Radiat. Res. 101*, 4−15.
16. Smith, S., Giriat, I., Schmitt, A., and de Lange, T. (1998) *Science 282*, 1484−1487.
17. Kickhoefer, V. A., Siva, A. C., Kedersha, N. L., Inman, E. M., Ruland, C., Streuli, M., and Rome, L. H. (1999) *J. Cell Biol. 146*, 917−928.
18. Eliasson, M. J., Sampei, K., Mandir, A. S., Hurn, P. D., Traystman, R. J., Bao, J., Pieper, A., Wang, Z. Q., Dawson, T. M., Snyder, S. H., and Dawson, V. L. (1997) *Nat. Med. 3*, 1089−1095.
19. Trucco, C., Oliver, F. J., de Murcia, G., and Menissier-de Murcia, J. (1998) *Nucleic Acids Res. 26*, 2644−2649.
20. Masutani, M., Suzuki, H., Kamada, N., Watanabe, M., Ueda, O., Nozaki, T., Jishage, K., Watanabe, T., Sugimoto, T., Nakagama, H., Ochiya, T., and Sugimura, T. (1999) *Proc. Natl. Acad. Sci. U.S.A. 96*, 2301−2304.
21. Jacobson, E. L., Smith, J. Y., Wielckens, K., Hilz, H., and Jacobson, M. K. (1985) *Carcinogenesis 6*, 715−718.
22. Szabo, C., and Dawson, V. L. (1998) *Trends Pharmacol. Sci. 19*, 287−298.
23. Ha, H. C., Juluri, K., Zhou, Y., Leung, S., Hermankova, M., and Snyder, S. H. (2001) *Proc. Natl. Acad. Sci. U.S.A. 98*, 3364−3368.
24. Lin, W., Amé, J. C., Aboul-Ela, N., Jacobson, E. L., and Jacobson, M. K. (1997) *J. Biol. Chem. 272*, 11895−11901.
25. Ying, W., Sevigny, M. B., Chen, Y., and Swanson, R. A. (2001) *Proc. Natl. Acad. Sci. U.S.A. 98*, 12227−12232.
26. Slama, J. T., Aboul-Ela, N., and Jacobson, M. K. (1995) *J. Med. Chem. 38*, 4332−4336.
27. Slama, J. T., Aboul-Ela, N., Goli, D. M., Cheesman, B. V., Simmons, A. M., and Jacobson, M. K. (1995) *J. Med. Chem. 38*, 389−393.
28. Ramsinghani, S., Koh, D. W., Amé, J. C., Strohm, M., Jacobson, M. K., and Slama, J. T. (1998) *Biochemistry 37*, 7801−7812.
29. Giner, H., Simonin, F., de Murcia, G., and Menissier-de Murcia, J. (1992) *Gene 114*, 279−283.
30. Thomassin, H., Jacobson, M. K., Guay, J., Verreault, A., Aboul-Ela, N., Ménard, L., and Poirier, G. G. (1990) *Nucleic Acids Res. 18*, 4691−4694.
31. Hatakeyama, K., Nemoto, Y., Ueda, K., and Hayaishi, O. (1986) *J. Biol. Chem. 261*, 14902−14911.
32. Chavan, A. J., Nemoto, Y., Narumiya, S., Kozaki, S., and Haley, B. E. (1992) *J. Biol. Chem. 267*, 14866−14870.
33. Edman, P., and Begg, G. (1967) *Eur. J. Biochem. 1*, 80−91.
34. Cline, J., Braman, J. C., and Hogrefe, H. H. (1996) *Nucleic Acids Res. 24*, 3546−3551.
35. Menard, L., and Poirier, G. G. (1987) *Biochem. Cell Biol. 65*, 668−673.
36. Kiehlbauch, C. C., Aboul-Ela, N., Jacobson, E. L., Ringer, D. P., and Jacobson, M. K. (1993) *Anal. Biochem. 208*, 26−34.
37. Jonsson, U., Fagerstam, L., Ivarsson, B., Johnsson, B., Karlsson, R., Lundh, K., Lofas, S., Persson, B., Roos, H., Ronnberg, I., et al. (1991) *BioTechniques 11*, 620−627.
38. Crestfield, A. M., Moore, S., and Stein, W. H. (1963) *J. Biol. Chem. 238*, 622−627.
39. Charbonneau, H. (1989) in *A Practical Guide to Protein and Peptide Purification for Microsequencing* (Matsudaira, P. T., Ed.) pp 15−30, Academic Press, New York.
40. King, S. M., Kim, H., and Haley, B. E. (1991) *Methods Enzymol. 196*, 449−466.
41. Brochu, G., Duchaine, C., Thibeault, L., Lagueux, J., Shah, G. M., and Poirier, G. G. (1994) *Biochim. Biophys. Acta 1219*, 342−350.
42. Braun, S. A., Panzeter, P. L., Collinge, M. A., and Althaus, F. R. (1994) *Eur. J. Biochem. 220*, 369−375.
43. Haley, B. E. (1991) *Methods Enzymol. 200*, 477−487.
44. Davies, G., and Henrissat, B. (1995) *Structure 3*, 853−859.

BI0272048